KSCE Journal of Civil Engineering (2017) 21(5):1706-1716

DOI 10.1007/s12205-016-0502-9

Geotechnical Engineering

pISSN 1226-7988, eISSN 1976-3808
www.springer.com/12205

Axisymmetric Passive Lateral Earth Pressure of Retaining Walls

Amin Keshavarz* and Mohsen Ebrahimi**

Received January 28, 2016/Revised July 12, 2016/Accepted September 7, 2016/Published Online November 11, 2016

Abstract

This paper attempted to examine the passive lateral earth pressure of axisymmetric retaining walls. The Stress Characteristics Method (SCM) was employed for analysis. The stress equilibrium equations were obtained through the finite difference method along the characteristic lines. Effects of backfill slope, wall angle, and radius of retaining wall on passive stress distribution on the retaining wall were analyzed. Furthermore, the wall was considered frictional and adhesive. Apart from the axisymmetric retaining wall, the analysis covered a wall under plane strain condition. The validity of the results was confirmed through developing and comparing a number of models through the finite element method versus the SCM. This study showed that the level of passive lateral pressure of retaining walls in axial symmetry was higher than that of walls under plane strain condition. Moreover, axial symmetry or plane strain type of wall did not affect the level of unconfined yield stress, which was evident in the finite element model.

Keywords: *stress characteristics method, passive earth pressure, axial symmetry, finite element method*

1. Introduction

Rigid retaining walls are abundantly applied to urban construction, road transport, harbor construction, etc. The passive pressure plays a key role in soil-structure interaction. The passive earth pressures are often adopted to enhance resistance to lateral movement of structures. It has always been a challenging task in geotechnical engineering to determine the level and distribution of passive earth pressure. Numerous studies have so far been conducted to specify the passive lateral earth pressure. Coulomb (1776) applied a theoretical solution to calculate earth pressure behind a retaining wall considering the soil-wall friction angle. He assumed the surface of rupture to be like a plane on which the frictional forces were distributed evenly. Moreover, Coulomb regarded earth as an isotropic and homogeneous material. Rankine (1857) also proposed a mathematical solution assuming the earth mass to be in plastic equilibrium. He defined the rupture condition according to Mohr-Coulomb soil model, proposing a formula for the passive earth pressure coefficient behind the frictionless retaining wall. Terzaghi (1943) developed a method for estimating the passive lateral earth pressure, assuming that the surface of rupture was composed of logarithmic spiral and straight plane. In addition to the three methods reviewed above, there are other methods concerning the limit equilibrium (Kumar, 2001; Kumar and Subba Rao, 1997; Patki *et al.*, 2015; Zhu and Qian, 2000). Based on the hypothesis of slip plane in earth pressure theory, Lu and Yuan (2011) proposed a new method for calculating the passive lateral pressure of cohesive earth based on Culmann's graphical method. Lots of studies are conducted on passive lateral pressure using limit analysis method (Chen, 1975; Chen and Liu, 1990; Soubra, 2000; Soubra and Macuh, 2002) and method of slices (limit equilibrium) (Chen and Li, 1998; Kumar and Subba Rao, 1997; Shields and Tolunay, 1973) to calculate the lateral earth pressure.

Initially proposed by Sokolovskii (1960; 1965), the Stress Characteristics Method (SCM) is ideal for estimating the lateral earth pressure. Furthermore, Graham (1971) made some numerical calculations for sand, and proposed the passive lateral pressure coefficient (K_p). Lee and Herington (1972) and Hettiaratchi and Reece (1975) developed a general equation based on SCM so as to estimate the passive lateral earth pressure. Kumar and Chitikela (2002) adopted SCM to estimate seismic lateral pressure coefficients of inclined retaining wall with non-cohesive backfill. Cheng (2003) used SCM for obtaining the values of active and passive lateral earth pressure in both static and seismic modes. Furthermore, Peng and Chen (2013) solved the slip line stress field through the stress characteristics method and determined the active earth pressure on retaining walls considering the effect of plastic critical depth. Using SCM, Keshavarz (2016) proposed a closed form solution to evaluate the plastic critical or tension crack depth of retaining walls in seismic case. This method has also been used in bearing capacity problems (Jahanandish and Keshavarz, 2005; Keshavarz *et al.*, 2016; Keshavarz *et al.*, 2011; Martin, 2005; Veiskarami *et al.*, 2011; Veiskarami *et al.*, 2014).

The values of lateral earth pressure on circular walls can be estimated by analyzing the lateral earth pressure problems in

*Assistant Professor, School of Engineering, Persian Gulf University, Bushehr, Iran (Corresponding Author, E-mail: keshavarz@pgu.ac.ir, amin_keshavarz@yahoo.com)
**Graduate Student, School of Engineering, Persian Gulf Universitym Bushehr, Iran (E-mail: mohsenebrahimi01@gmail.com)

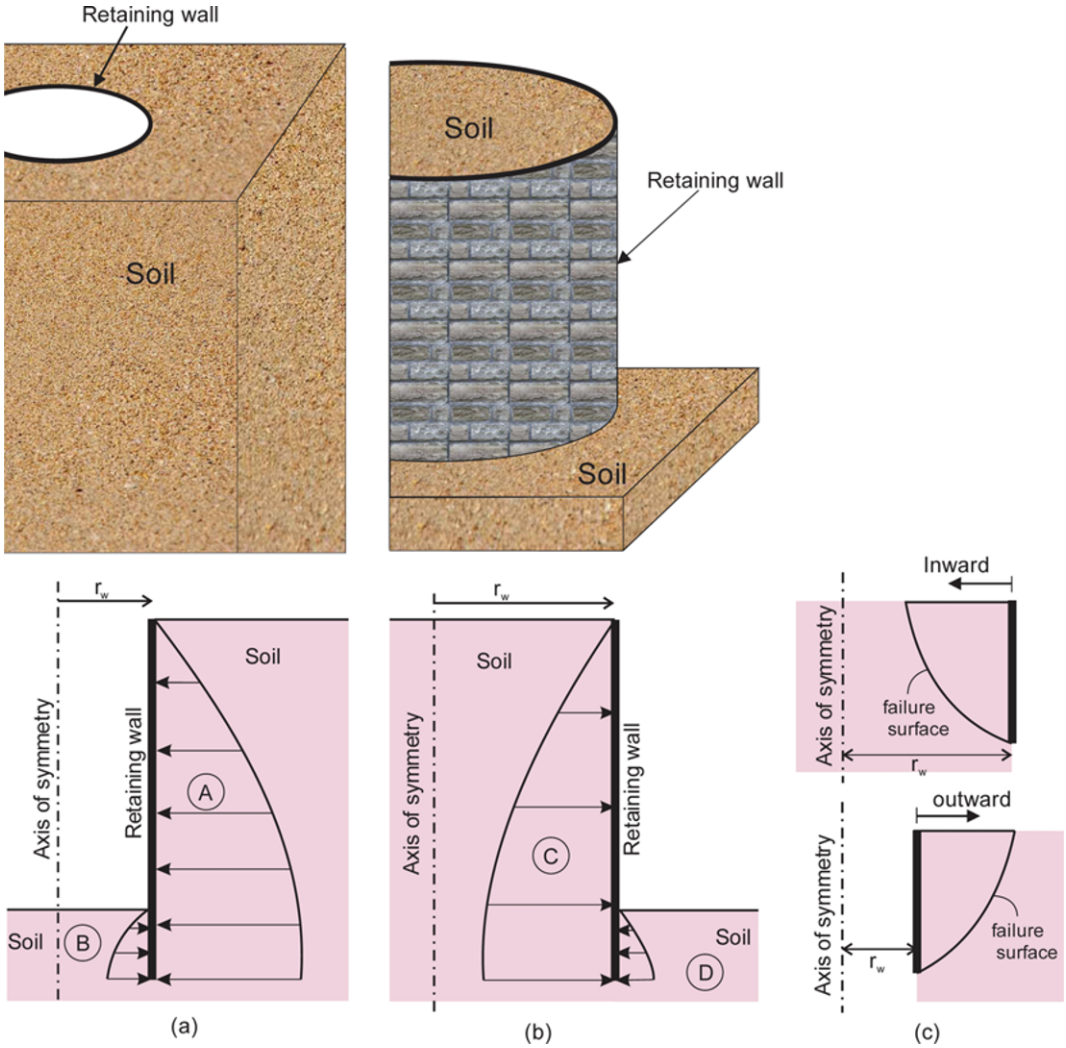

Fig. 1. Types of the Retaining Walls in Axisymmetric Condition: (a) Case A, (b) Case B, (c) Inward and Outward Mechanisms

axial symmetry. The axisymmetric walls vary in radius, greater levels of which can obviously render analytical results in axial symmetry approximate to the results obtained under plane strain condition. Several researchers applied SCM solution to problems of active lateral earth pressure in axial symmetry (Berezantzev, 1958; Cheng *et al.*, 2008; Cheng *et al.*, 2007; Keshavarz and Ebrahimi, 2016; Liu, 2014; Liu and Wang, 2008; Liu *et al.*, 2008, 2009a, 2009b).

Figure 1 shows two types of retaining walls in axisymmetric condition. Case A (Fig. 1(a)) is used in circular excavations, vertical shafts, etc. However, case B (Fig. 1(b)) is widely used in highway constructions, grain silos and other geotechnical structures. In Fig. 1(a), when the retaining wall moves enough toward the axis of symmetry, point A and point B will be in the active and passive cases, respectively. Likewise, in case B (Fig. 1(b)), when the wall moves away from the axis of symmetry, active and passive states can be occurred in points C and D, respectively. Throughout this paper, for the passive earth pressure, the inward mechanism indicates the case where the retaining wall moves toward the axis of symmetry, and passive failure zone is created between the wall and axis of symmetry (Fig. 1(c)). In the outward mechanism, wall moves away from the axis of symmetry (Fig. 1(c)).

In previous studies, researchers showed that it was too conservative to adopt the results of plane strain for analysis of retaining walls in axial symmetry, whereas the plane strain analysis reflected greater active lateral pressure outputs as compared to the axial symmetry analysis (Cheng *et al.*, 2007; Liu and Wang, 2008). The stress characteristics method has so far been adopted by numerous research projects to determine the active and passive lateral earth pressures under static and seismic conditions for retaining walls under plane strain condition, even though it has never been employed to estimate the passive lateral earth pressure in analysis of retaining walls at axial symmetry mode. Moreover, the passive lateral pressure in axial symmetry has not been addressed by other methods. In this paper, the values of passive lateral earth pressure and lateral pressure coefficient were estimated for retaining walls at both axial symmetry and plane strain. The backfill was angled, frictional and cohesive and complies with the Mohr-Coulomb rupture criterion. The wall was rigid and

angled. The friction angle and adhesion were considered to be between soil and wall.

2. Theory

For a soil element in axial symmetry (Fig. 2), the equilibrium equations in the differential form are

$$\frac{\partial \sigma_r}{\partial r}+\frac{\partial \tau_{rz}}{\partial z}=f_r$$
$$\frac{\partial \sigma_z}{\partial z}+\frac{\partial \tau_{rz}}{\partial r}=f_z \quad (1)$$

where

$$f_r=-\frac{n}{r}(\sigma_r-\sigma_\theta)$$
$$f_z=-\gamma-\frac{n}{r}\tau_{rz} \quad (2)$$

Moreover, $n = 0$ and $n = 1$ were related to plane strain and axial symmetry, respectively and γ is the unit weight of the soil. The values of σ_θ based on Haar and Karman's hypothesis (Haar and Karman, 1909) in axial symmetry for the passive case are σ_1 and σ_3 for the inward and outward walls, respectively. The Haar-von Karman hypothesis has been very widely used to solve problems in axisymmetric case. There is no evidence indicating the actual state of the intermediate principal stress and in fact, there is always a lack of information about the circumferential stress; however, to keep it always within an admissible range, one should choose either the minor or the major principal stress (or something between). The selected choice in this study is indeed a safe choice. The results of the experimental study and discrete element method (Tobar and Meguid, 2011; Tran *et al.*, 2012) have demonstrated a good agreement with the solutions obtained using Harr-Karman's hypothesis such as Terzaghi (1943), Berezantzev (1958) and Liu *et al.* (2009b).

If p represents the mean stress equivalent to $(\sigma_r+\sigma_z)/2$ and ψ is the angle between r axis and the direction of major principal stress (σ_1) within the Mohr's circle, then the stress components are formulated as follows:

$$\sigma_r=p(1+\sin\phi\cos 2\psi)+c\cos\phi\cos 2\psi$$
$$\sigma_z=p(1-\sin\phi\cos 2\psi)-c\cos\phi\cos 2\psi$$
$$\tau_{rz}=(p\sin\phi+c\cos\phi)\sin 2\psi \quad (3)$$

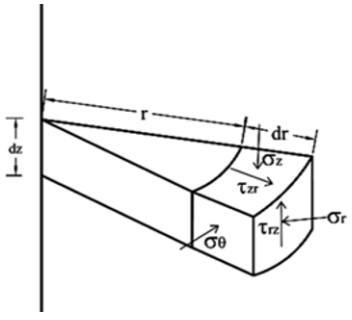

Fig. 2. Soil Element in Axial Symmetry Mode

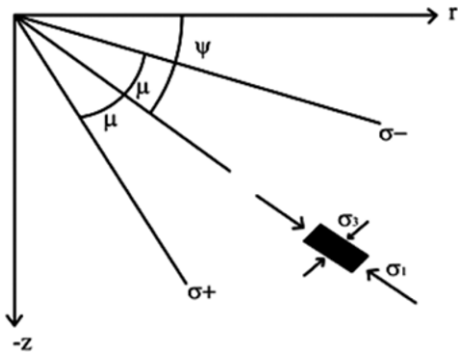

Fig. 3. Direction of Stress Characteristic Lines

where c and ϕ are the cohesion and friction angle of the soil. Fig. 3 illustrates the direction of characteristic lines on a soil element, where the two directions are called positive and negative characteristics. The characteristic lines and maximum principal stress axis (σ_1) constitute the $\mu = \pi/4\text{-}\phi/2$ angle. The slope of positive and negative stress characteristic lines is determined as follows (Fig. 3):

$$\text{Along the positive direction } (\sigma^+): \quad \frac{dz}{dr}=\tan(\psi+\mu)$$
$$\text{Along the negative direction } (\sigma^-): \quad \frac{dz}{dr}=\tan(\psi-\mu) \quad (4)$$

Through derivations of Eq. (3) and inserting them in stress equilibrium Eqs. (1) and after reducing them, the equations will be formulated along the positive and negative characteristic lines as follows:

$$dp+2(p\tan\phi+c)d\psi=f_r(dr-\tan\phi dz)+f_z(\tan\phi dr+dz)$$
$$dp-2(p\tan\phi+c)d\psi=f_r(dr+\tan\phi dz)+f_z(-\tan\phi dr+dz) \quad (5)$$

If BC and AC are positive and negative characteristic lines, respectively and the values of r, z, p and ψ are known at points A and B, the properties of point C (r_C, z_C, p_C and ψ_C) can be found through simultaneous solution of the finite difference forms of Eqs. (4) and (5). The values of r_C and z_C are determined first by writing the finite difference form of Eq. (4) as follows:

$$\text{for } \sigma^+: \frac{z_C-z_B}{r_C-r_B}=0.5\left(\tan(\psi_C+\mu)+\tan(\psi_B+\mu)\right)=t_{mp}$$
$$\text{for } \sigma^-: \frac{z_C-z_A}{r_C-r_A}=0.5\left(\tan(\psi_C-\mu)+\tan(\psi_A-\mu)\right)=t_{mm} \quad (6)$$

Then, the values of r_C and z_C can be determined as follows:

$$r_C=\frac{z_A-z_B-r_A t_{mm}+r_B t_{mp}}{t_{mp}-t_{mm}}$$
$$z_C=(r_C-r_B)t_{mp}+z_B \quad (7)$$

The values of p_C and ψ_C were determined by formulating Eq. (5) as finite difference as follows:

$$\text{for } \sigma^+: \ (p_C-p_B)+B_{mp}(\psi_C-\psi_B)=C_{mp}+D_{mp}$$
$$\text{for } \sigma^-: \ (p_C-p_A)+B_{mm}(\psi_C-\psi_A)=C_{mm}+D_{mm} \quad (8)$$

where,

$$
\begin{aligned}
B_{mp} &= \left(p_C + p_B\right)\tan\phi + 2c \\
B_{mm} &= -\left(p_C + p_A\right)\tan\phi - 2c \\
C_{mp} &= 0.5\left(f_{rC} + f_{rB}\right)\left[\left(r_C - r_B\right) - \left(z_C - z_B\right)\tan\phi\right] \\
C_{mm} &= 0.5\left(f_{rC} + f_{rA}\right)\left[\left(r_C - r_A\right) + \left(z_C - z_A\right)\tan\phi\right] \\
D_{mp} &= 0.5\left(f_{zC} + f_{zB}\right)\left[\left(r_C - r_B\right)\tan\phi + \left(z_C - z_B\right)\right] \\
D_{mp} &= 0.5\left(f_{zC} + f_{zA}\right)\left[-\left(r_C - r_A\right)\tan\phi + \left(z_C - z_A\right)\right]
\end{aligned}
\tag{9}
$$

By solving Eq. (8), the values of p_C and ψ_C can be determined as follows:

$$
\begin{aligned}
\psi_C &= A_1 / A_2 \\
p_C &= p_B + C_{mp} + D_{mp} - B_{mp}\left(\psi_C - \psi_B\right)
\end{aligned}
\tag{10}
$$

where,

$$
\begin{aligned}
A_1 &= p_B - p_A + C_{mp} + D_{mp} + B_{mp}\psi_B - B_{mm}\psi_A - C_{mm} - D_{mm} \\
A_2 &= B_{mp} - B_{mm}
\end{aligned}
\tag{11}
$$

Finally, Eqs. (7) and (10) as well as the iterative solution were adopted to obtain the unknown values at C.

2.1 Boundary Conditions

To start the analysis and solve the characteristics network in all geotechnical issues, the boundary conditions should first be determined. Fig. 4 specifies the geometry of the retaining wall problem in passive case. ODA is the rupture zone specified by solving the stress characteristics network. OD represents the earth boundary making β angle with the horizontal axis, where the surcharge q is vertically applied. The wall makes θ angle with the vertical axis. Angles β and θ are positive counter-clockwise.

If the earth boundary is assumed to have a length of L divided into n number of nodes, the coordinates of each node on the ground surface can be determined from the geometry of the problem. The values of p and ψ on the ground surface shall be determined with regard to the values of the applied stress. Hence, the values of normal (σ_0) and shear (τ_0) stresses are first determined as:

$$
\begin{aligned}
\sigma_0 &= q\cos^2\beta \\
\tau_0 &= q\cos\beta\sin\beta
\end{aligned}
\tag{12}
$$

Figure 5(a) illustrates the Mohr's circle on the ground surface, where the radius can be determined as:

$$
R_0 = \sqrt{\left(p_0 - \sigma_0\right)^2 + \tau_0^2} = p_0\sin\phi + c\cos\phi \tag{13}
$$

At the end, the values of p_0 can be expressed as:

$$
p_0 = \frac{\sigma_0 + \left(c\cos\phi\sin\phi\right) + \sqrt{\left(\sigma_0\sin\phi + c\cos\phi\right)^2 - \left(\tau_0\cos^2\phi\right)^2}}{\cos^2\phi} \tag{14}
$$

Regarding Mohr's stress circle (Fig. 5(a)):

$$
\begin{aligned}
\psi_0 &= \eta + \beta \\
\sigma_0 &= p_0 - R_0\cos 2\eta \\
\tau_0 &= R_0\sin 2\eta
\end{aligned}
\tag{15}
$$

According to Eqs. (12) and (15), the value of ψ_0 is determined as follows:

$$
\begin{aligned}
\psi_0 &= 0.5\left(\beta + \arcsin\left(\frac{p_0\sin\beta}{p_0\sin\phi + c\cos\phi}\right)\right) && \text{if } q \neq 0 \\
\psi_0 &= \beta && \text{if } q = 0
\end{aligned}
\tag{16}
$$

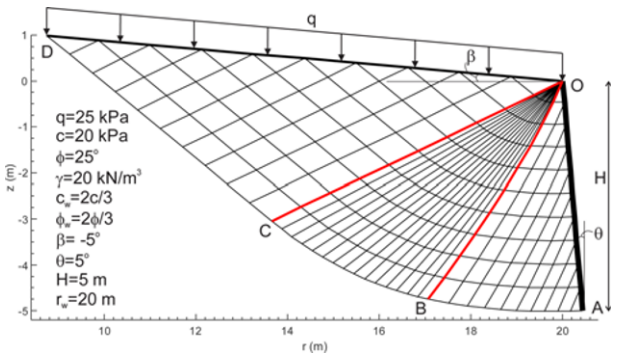

Fig. 4. Geometry of the Problem and Sample of the Characteristics Network for Inward Mechanism

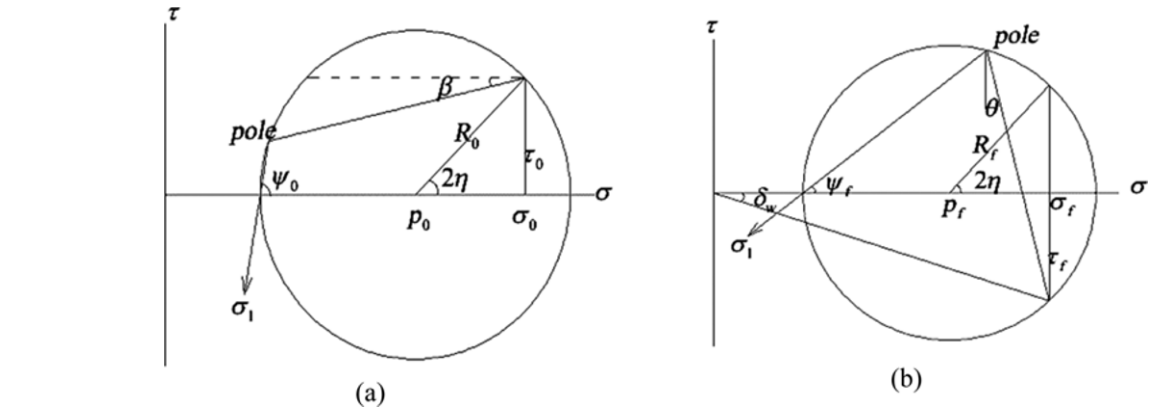

Fig. 5. Mohr's Stress Circle for the Retaining Wall in Passive Case: (a) on the Ground Boundary, (b) Along the Retaining Wall

By drawing Mohr's stress circle at the retaining wall boundary (Fig. 5(b)), the following equations can be formulated:

$$\begin{aligned}&\psi_f = \eta + \theta\\ &\sigma_f = p_f + R_f \cos 2\eta\\ &\tau_f = c_w + \sigma_f \tan\delta_w = R_f \sin 2\eta\\ &R_f = p_f \sin\phi + c\cos\phi\end{aligned} \tag{17}$$

where δ_w and c_w represent friction angle and adhesion of the soil-wall interface, respectively. Finally by solving Eq. (17), the value of ψ_f on the retaining wall boundary is determined as:

$$\psi_f = \theta + 0.5\left(\delta_w + \arcsin\left(\frac{p_f \sin\delta_w + c_w \cos\delta_w}{p_f \sin\phi + c\cos\phi}\right)\right) \tag{18}$$

2.2 Analysis Procedure

The characteristic lines network should be solved to determine passive stress applied by earth to the wall. An example of characteristics network can be seen in Fig. 4. Increase in the number of nodes can enhance the accuracy in calculation of passive stress. Moreover, a computer code was written so as to create a network. This code draws the characteristics network and determines the output parameters concerning pressure distribution and passive force exerted on the wall by adopting the input parameters such as properties of soil, wall, geometry of the wall, etc. The analysis trend varied according to the values of ψ_0 and ψ_f, which may occur in the following three modes:

1- $\psi_f > \psi_0$: If the value of ψ angle at the retaining wall boundary is greater than that on the ground surface, the characteristics network would cover three zones of Rankine (ODC), Goursat (OCB) and Mixed (OBA). The characteristics network was determined firstly through specifying the boundary conditions for points on the ground surface (r, z, p_0 and ψ_0). Then, the two points A and B with known parameters, the unknown values for point C are obtained through Eqs. (7) and (10). This procedure is repeated until all the Rankine points are specified.

At the next stage, point O is resolved. Because the values of stress on the right and left sides of this point are not the same, it is regarded as a singularity point, as formulated below. In this point, dr = dz = 0. If the very small zone around this point is divided into m parts (Fig. 6), the value of ψ for i-th component can be determined as follows:

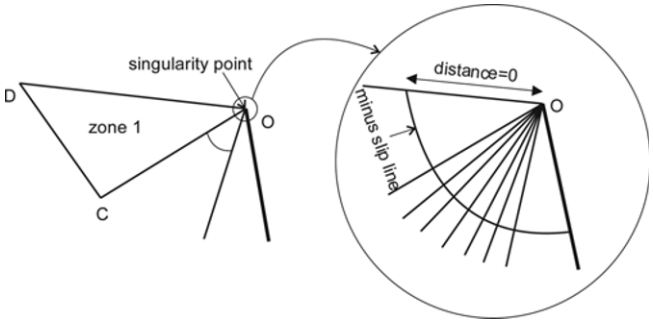

Fig. 6. Solving the Singularity Point

$$\psi_i = \psi_0 + i\left(\psi_f - \psi_0\right)/m \tag{19}$$

The stress equilibrium equation on the negative characteristic line is determined through Eq. (5). Finally, the value of p is determined based on Eq. (5) as:

$$\mathrm{d}p - 2\left(p\tan\phi + c\right)\mathrm{d}\psi = 0 \tag{20}$$

$$\begin{aligned}&p_i = p_0 + 2c\left(\psi_i - \psi_0\right) && \text{if } \phi = 0\\ &p_i = -c\cot\phi + \left(p_0 + c\cot\phi\right)\exp\left(2\tan\phi\left(\psi_i - \psi_0\right)\right) && \text{if } \phi \neq 0\end{aligned} \tag{21}$$

After solving the singularity point O, using the parameters of points on OC and the 3-point strategy, the Goursat zone is solved. Afterwards, the parameters of points on OB, 3-point strategy and the wall boundary conditions were employed to solve Mixed zone.

2- $\psi_0 = \psi_f$: If the values of ψ at the retaining wall boundary and ground surface are equal, the characteristics network will include Rankine and Mixed zones and exclude Goursat zone. In this scenario, the Rankine zone is solved directly without involving the singularity point and using the parameters of boundary points OB (or OC), the stress equilibrium equations and boundary conditions on the wall, Mixed zone was solved.

3- $\psi_0 > \psi_f$: In this mode where the values of ψ at the retaining wall boundary are lower than those on the earth boundary, Goursat zone is excluded and Rankine and Mixed zones were converged leading to a discontinuity line in the stress field. The Lee and Herington's method (Lee and Herington, 1972) was modified for solving the characteristics network. Then, it was used to analyze the retaining wall.

2.3 Finite Element Modeling

Finite element analysis is a suitable method for analyzing geotechnical problems. It can solve the partial differential equations numerically. In this paper, the accuracy of the results was confirmed through the PLAXIS, a software application for Finite Element Method (FEM). Similarly, Yang and Liu (2007) and Yap *et al.* (2012) applied the same software to determine the active lateral earth pressure under plane strain condition. Table 1 and Fig. 7 illustrate the parameters and sample model developed for a circular retaining wall. The modeling involved standard fixity and 15-node fine-mesh elements. The beam was employed as an element to create a rigid retaining wall. Moreover, a minimum prescribed displacement was applied to the wall (Fig. 7) so as to provide a passive state and rupture in the earth.

Table 1. Parameters used in Finite Element Modeling

	Parameter	Value
Soil properties	Soil unit weight γ(kN/m^3)	20
	Elastic modulus E (kPa)	3.0E+4
Material properties for rigid retaining wall	Bending stiffness EI (kN.m^2)	2.5E+6
	Normal stiffness EA (kN)	3.0E+7
	Poisson Ratio υ	0.2

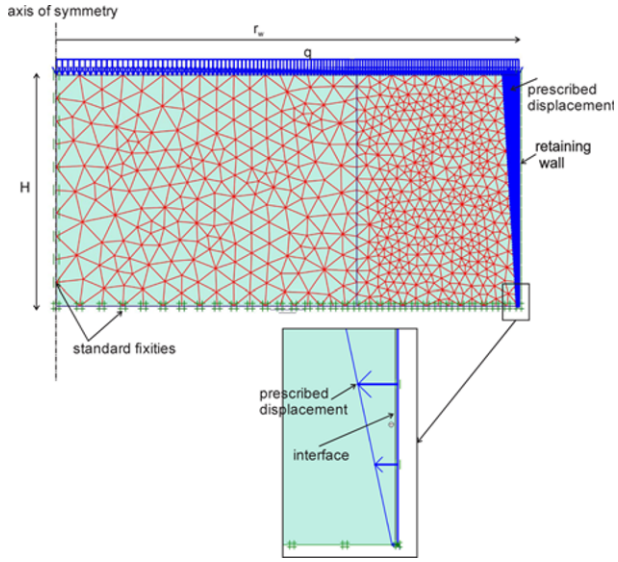

Fig. 7. Inward Model Prototype of FEM

3. Discussions and Parametric Studies

The parameters involved in the analysis, such as the internal friction angle (ϕ), soil angle (β) and so on are effective in the form of characteristics network, earth rupture zone and stress distribution exerted on the wall. This section explores the effect of these parameters. It should be noted that unlike the active mode, the stress value is not negative on the ground surface in the passive mode, but there is a minimum horizontal stress, the level of which can be obtained through Eq. (22):

$$f_c = 2c\sqrt{K_p} \tag{22}$$

where f_c represents the unconfined yield stress, exerting the maximum compressive stress on free ground surface, K_p is the coefficient of passive lateral earth pressure equal to $P_p/(0.5\gamma H^2)$, where P_p is the passive lateral force. In the examples provided in this section, the values of f_c and its variations can be obtained according to the figures.

Figure 8 displays the impact of retaining wall radius on the stress distribution exerted on the axisymmetric inward and outward retaining walls. According to this figure, with an increase of wall radius, the passive lateral pressure exerted on the wall will decrease. The level of passive lateral pressure in r_w = 1000 m mode is approximate to that for a similar retaining wall under plane strain condition. The values of this parameter at the bottom of the wall in r_w = 1000 m in outward, inward and plane strain cases are 634.1, 630.3 and 629.5 kPa, respectively.

Figure 9 and Fig. 10 show the impact of ground surface angle (β) on stress distribution and earth rupture zone, respectively. As the ground angle grows from 0 to -25 degrees, the level of passive lateral pressure across the walls steadily increases by 35.9 and 67.4% at the bottom of the inward and outward walls, respectively. Furthermore, as the ground surface angle grows from 0 to -25 degrees, the length of the rupture zone on the

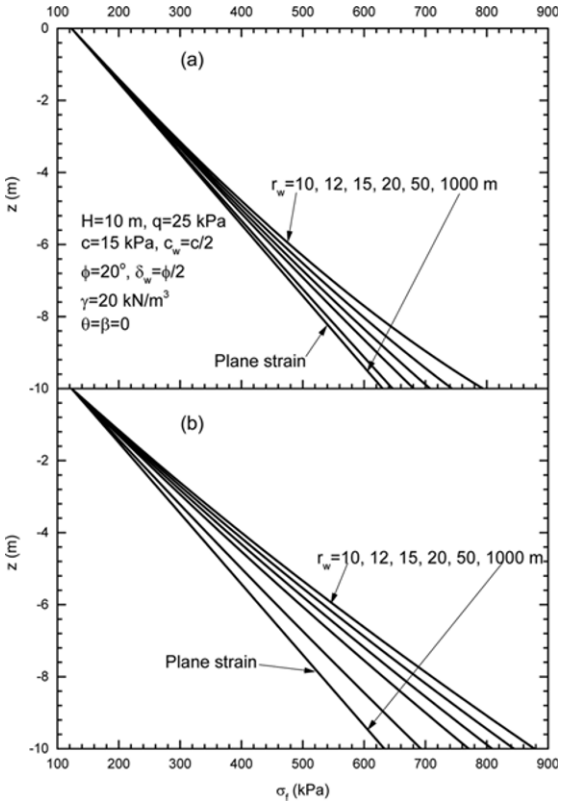

Fig. 8. Effect of Wall Radius on Stress Distribution in: (a) Inward, (b) Outward Mechanisms

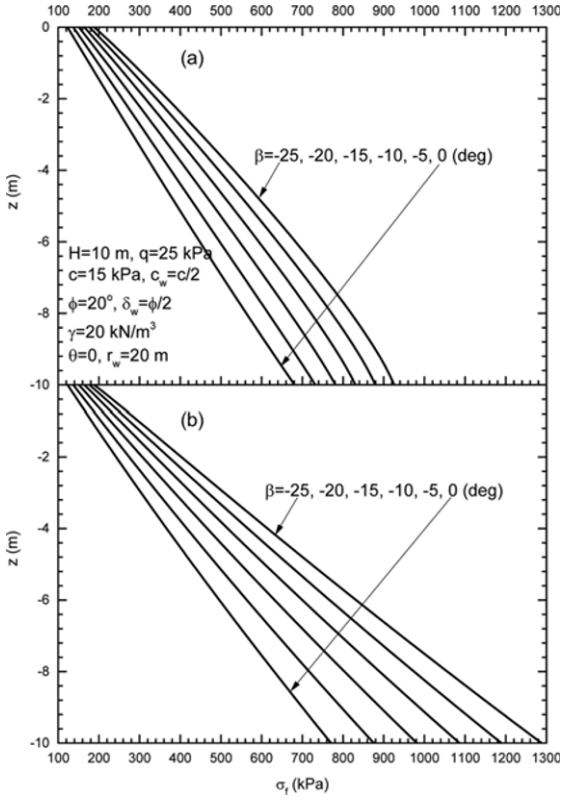

Fig. 9. Impact of Ground Surface Angle (β) on Stress Distribution in: (a) Inward, (b) Outward Mechanisms

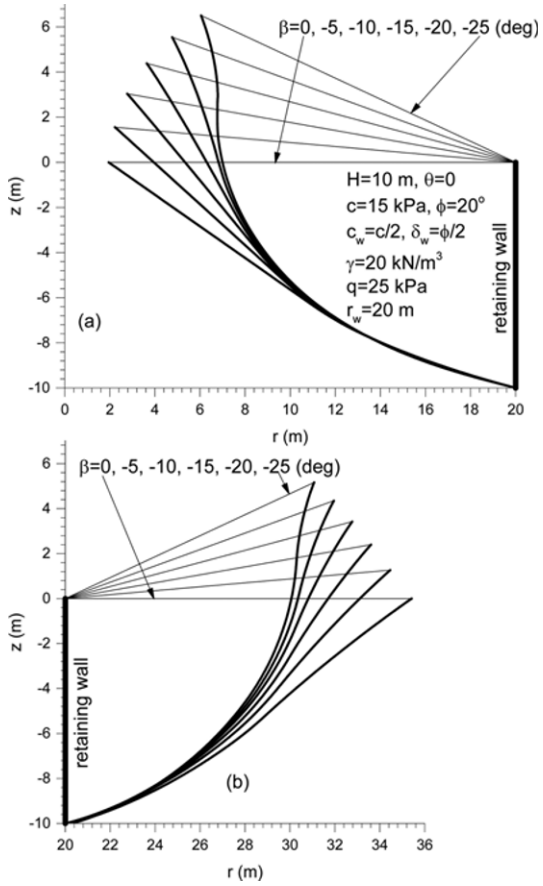

Fig. 10. Impact of Ground Surface Angle (β) on Earth Rupture Zone in: (a) Inward, (b) Outward Mechanisms

ground surface curtails by about 22.7 and 28.2% in the axisymmetric inward and outward walls, respectively.

Figure 11 displays the impact of wall angle (θ) on the stress distribution exerted by earth. As the wall angle grows from 0 to -20, the passive lateral pressure steadily decreases by 30.8 and 28.3% at the bottom of the inward and outward walls, respectively. The studies on the impact of the wall angle on the rupture zone revealed that the rupture zone is slightly altered by variations in the wall angle. It should be noted that variations in ground surface and wall angles were considered to be in direction where they were more likely to occur. Fig. 12 and Fig. 13 illustrate the effect of friction angle (δ_w) and adhesion (c_w) of the soil-wall interface, respectively. The results indicated that as δ_w increases from 0 to ϕ, the unconfined yield stress (f_c) and stress value at the bottom of the wall increased by 31.6 and 59.3 percent in the inward wall and 31.6 and 42.0 percent in the outward wall, respectively. Nevertheless, as c_w grows from 0 to c, f_c and stress at the bottom of the wall increase by 10.2 and 4.1 percent in the inward wall and 10.2 and 2.5 percent in the outward wall, respectively. Fig. 14 displays the effect of earth internal friction angle (ϕ) on the stress distribution. As ϕ increases, the earth passive lateral pressure increases. The effect of this parameter is remarkable on the pressure exerted onto the retaining wall.

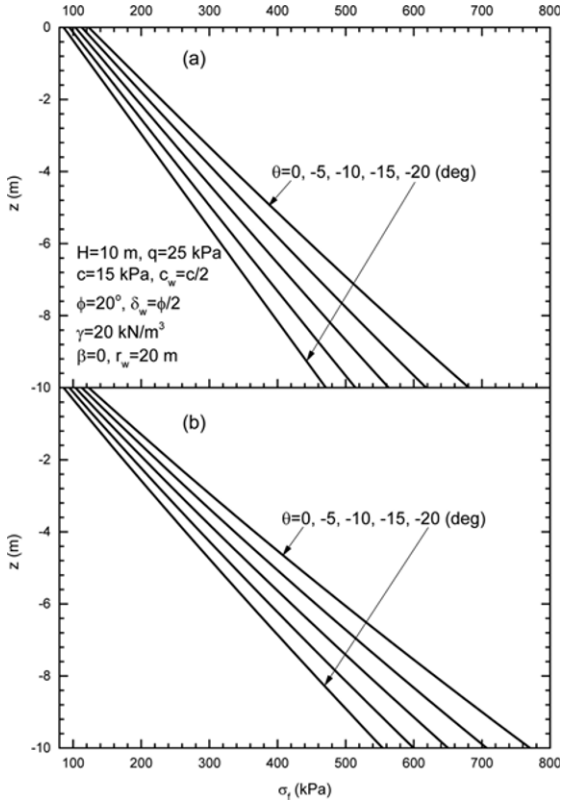

Fig. 11. Impact of Wall Angle (θ) on Stress Distribution in: (a) Inward, (b) Outward Mechanisms

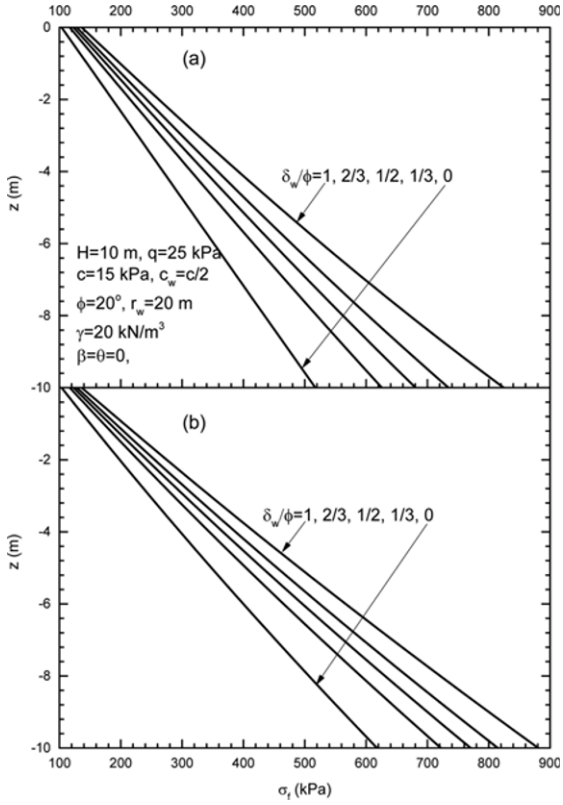

Fig. 12. Impact of Soil-wall Interface Friction Angle (δ_w) on stress distribution in: (a) Inward, (b) Outward Mechanisms

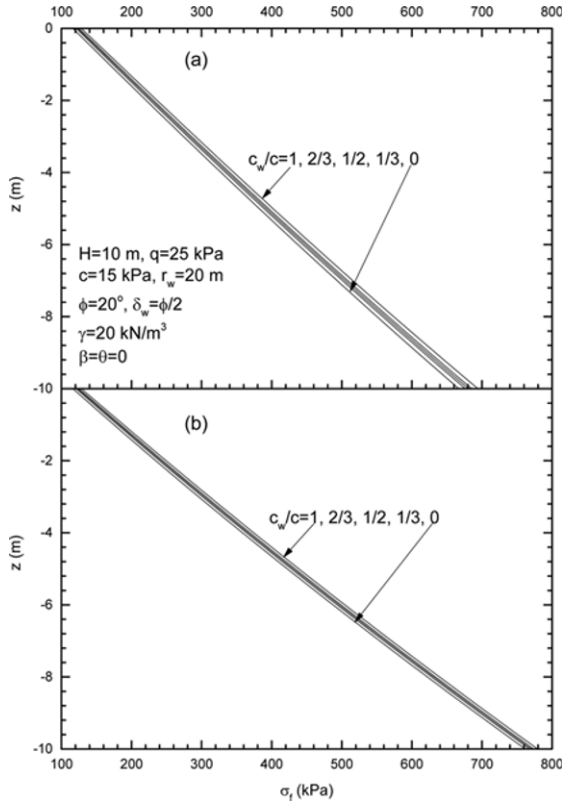

Fig. 13. Impact of Soil-wall Interface Adhesion (c_w) on Stress Distribution in: (a) Inward, (b) Outward Mechanisms

4. Comparisons

In previous section, the studies showed that the results of passive lateral pressure in axial symmetry were larger than those under plane strain condition. Fig. 15 compares the results of finite element and those of passive stress distribution exerted on the axisymmetric retaining walls with a radius of 20 m and plane strain in SCM. Fig. 15(a) and Fig. 15(b) show the stress distribution at different ratios of wall friction angle and adhesion. The comparison of results showed an adequate consistency between the finite element method and stress characteristics method. The finite element model reveals an irregularity in stress distribution at the bottom of the wall. Furthermore, the results indicated that the type of retaining wall (circular or plane strain) has no effect on the level of f_c, but most affect the level of stress at the bottom of the wall.

A comparison between the SCM failure surface and FEM incremental shear strain contour is prepared in Fig. 16. As clearly seen, the SCM failure surfaces pass through the maximum incremental shear strain zone for both inward and outward walls.

In order to ensure validity of the results, Table 2 compares the passive lateral earth pressure coefficient $K_{p\gamma}$ for the axisymmetric inward and outward retaining wall with a height of 5 m at various radii and the results of plane strain condition discussed in this paper and other relevant studies. It should be noted that the results of lateral pressure coefficients in analysis of the axisymmetric retaining walls depend on the height of the wall.

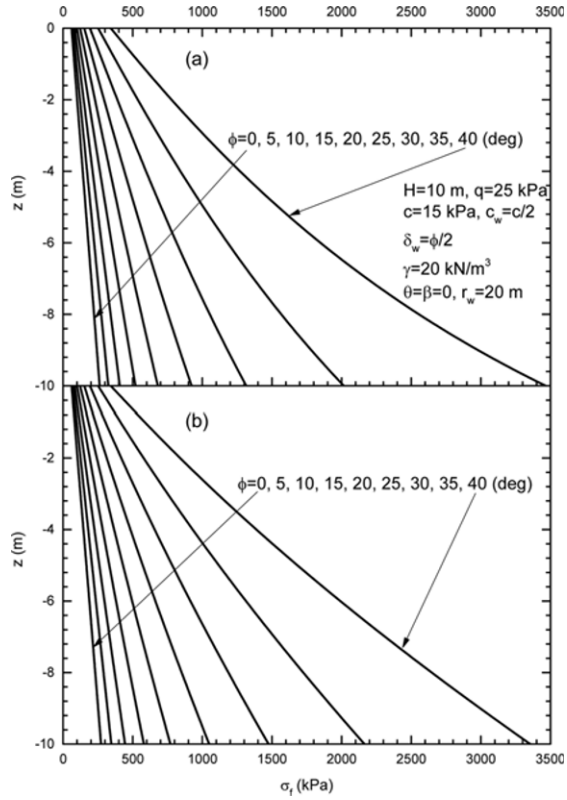

Fig. 14. Impact of Soil Internal Friction Angle (ϕ) on Stress Distribution in: (a) Inward, (b) Outward Mechanisms

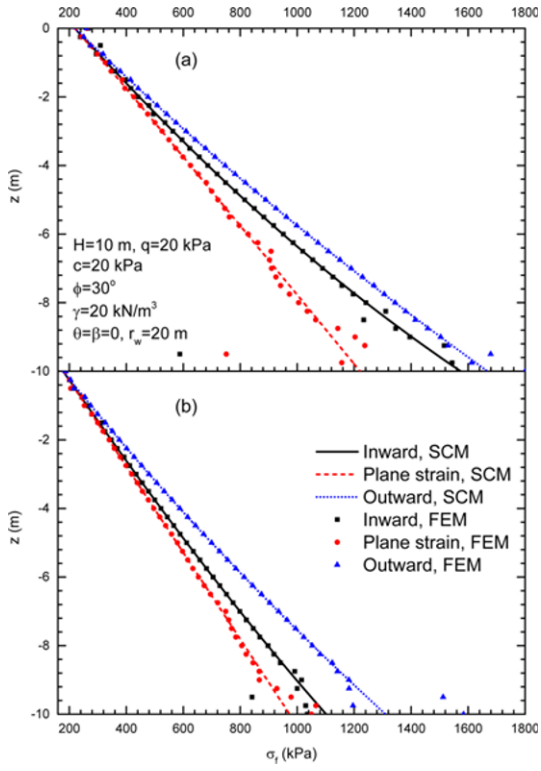

Fig. 15. Comparison of Results Obtained from SCM and FEM for: (a) $\delta_w = 2\phi/3$ and $c_w = 2c/3$, (b) $\delta_w = \phi/3$ and $c_w = c/3$

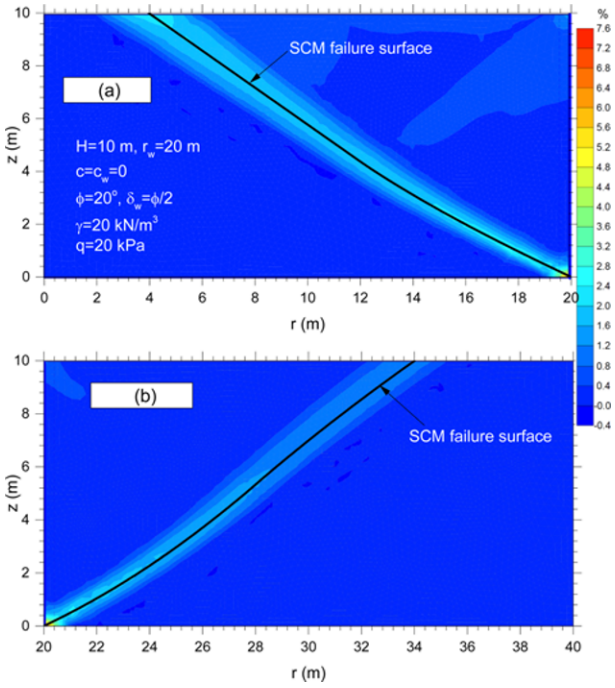

Fig. 16. Comparison between the SCM Failure Surface and FEM Incremental Shear Strain Contour for: (a) Inward, (b) Outward Mechanisms

According to Table 2, as the radius of the axisymmetric retaining wall increases, the results will be approximate to plane strain. In fact, the difference between the results of plane strain and axisymmetric retaining wall at r_w = 10 and 1000 m are averagely 17.3 and 0.4 percent in the outward wall and 10.8 and 0.1 percent in the inward wall, respectively, in all the ϕ and δ_w values. Furthermore, the comparison between the results of plane strain and those obtained by other researchers suggested that the highest and lowest consistency of results was related to that of Kumar and Subba Rao (1997) and Coulomb respectively, with 0.03 and 16.1% inconsistency. Table 3 compares the lateral earth pressure coefficient $K_{p\gamma}$ considering the variation in the wall angle (θ). It should be noted that the results for the axisymmetric wall were recorded with a height of 5 meters, where the inconsistencies of plane strain results obtained by Lee and Herington (1972) and Chen (1975) were averagely 0.02 and 6.8%, respectively, in all the ϕ and θ values.

5. Conclusions

The passive lateral earth pressure obtained by analyzing retaining wall under plane strain condition was invariably lower than that in analysis of retaining wall under axial symmetry. With

Table 2. Comparison of $K_{p\gamma}$ and other methods in $\beta = \theta = 0$

		$\phi = 20^o$		$\phi = 30^o$		$\phi = 40^o$	
Type of Wall		$\delta_w = \phi/3$	$\delta_w = 2\phi/3$	$\delta_w = \phi/3$	$\delta_w = 2\phi/3$	$\delta_w = \phi/3$	$\delta_w = 2\phi/3$
Outward	r_w = 10 m	2.66	3.07	4.81	6.37	9.85	16.36
	r_w = 20 m	2.53	2.91	4.43	5.85	8.78	14.46
	r_w = 100 m	2.42	2.77	4.11	5.38	7.83	12.72
	r_w = 1000 m	2.39	2.74	4.03	5.27	7.60	12.29
Inward	r_w = 10 m	2.44	2.87	4.26	5.95	8.71	16.84
	r_w = 20 m	2.41	2.79	4.12	5.55	8.04	13.96
	r_w = 100 m	2.39	2.74	4.04	5.31	7.65	12.52
	r_w = 1000 m	2.38	2.73	4.02	5.26	7.58	12.26
Plane strain	This study	2.38	2.73	4.02	5.26	7.57	12.23
	Coulomb	2.41	2.89	4.54	6.11	8.15	18.70
	Kérisel and Absi (1990)	2.40	2.75	4.00	5.30	7.60	12.00
	Kumar and Subba Rao (1997)	2.38	2.73	4.02	5.26	7.58	12.24
	Soubra and Macuh (2002)	2.39	2.75	4.03	5.34	7.62	12.60
	Patki *et al.* (2015)	2.39	2.75	4.03	5.34	7.62	12.60
	Reddy *et al.* (2013)	2.40	2.85	4.05	5.57	7.62	13.27

Table 3. Comparison of $K_{p\gamma}$ and Other Methods in $\delta_w = 0$ and $\beta = 0$

Type of Wall		$\theta = 0$		$\theta = -10^o$		$\theta = -20^o$	
		$\phi = 30^o$	$\phi = 40^o$	$\phi = 30^o$	$\phi = 40^o$	$\phi = 30^o$	$\phi = 40^o$
Outward	r_w = 20 m	7.35	22.35	5.74	15.03	4.72	10.80
	r_w = 100 m	6.74	19.62	5.31	13.32	4.39	9.68
	r_w = 1000 m	6.59	18.92	5.20	12.88	4.30	9.38
Inward	r_w = 20 m	7.13	23.69	5.49	14.94	4.46	10.32
	r_w = 100 m	6.69	19.61	5.24	13.17	4.32	9.51
	r_w = 1000 m	6.58	18.91	5.19	12.86	4.30	9.36
Plane strain	This study	6.57	18.84	5.19	12.83	4.30	9.35
	Lee and Herington (1972)	6.55	18.60	5.26	12.80	4.32	9.36
	Chen (1975)	7.10	20.90	5.46	13.90	4.41	9.88

increase of the radius of circular retaining wall, the results of both analyses become consistent. The computer code written for the stress characteristics method analyzed the axisymmetric retaining walls and walls under plane strain condition. This paper intended to examine the effect of soil-wall interface adhesion and friction angle, ground surface slope and wall angle on the axisymmetric retaining walls. At the end, the results were validated by determining the passive lateral pressure and passive lateral pressure coefficient at various radii, which were then compared with the results of plane strain. In previous section, the studies indicated that as the internal friction angle (ϕ) and wall friction angle (δ_w) increase, there will be greater difference between the results of circular retaining walls and plane strain condition. Hence, it is more desirable to conduct such analyses under axial symmetry conditions. In smaller internal friction angles, however, the difference between the two analyses drops as the plane strain analysis can be conservatively employed instead of the axial symmetry mode. The results were juxtaposed through various FEM modeling, the results of which were then compared with those obtained by the SCM, revealing a desirable level of consistency.

References

Berezantzev, V. (1958). "Earth pressure on the cylindrical retaining walls." *Conference on Earth Pressure Problems, Brussels.*

Chen, W. (1975). "Limit analysis and soil plasticity." *Elsevier: Amsterdam*.

Chen, W. and Liu, X. (1990). "Limit analysis in soil mechanics." *Developments in Geotechnical Engineering*, Vol. 52, Elsevier.

Chen, Z. and Li, S. (1998). "Evaluation of active earth pressure by the generalized method of slices." *Canadian Geotechnical Journal,* Vol. 35*,* No. 4, pp. 591-599, DOI: 10.1139/t98-022.

Cheng, Y. (2003). "Seismic lateral earth pressure coefficients for c–φ soils by slip line method." *Computers and Geotechnics,* Vol. 30*,* No. 8, pp. 661-670, DOI: 10.1016/j.compgeo.2003.07.003.

Cheng, Y., Au, S., Hu, Y., and Wei, W. (2008). "Active pressure for circular cut with berezantzev's and prater's theories, numerical modeling and field measurements." *Soils and Foundations,* Vol. 48*,* No. 5, pp. 621-631, DOI: 10.3208/sandf.48.621.

Cheng, Y., Hu, Y., and Wei, W. (2007). "General axisymmetric active earth pressure by method of characteristics—theory and numerical formulation." *International Journal of Geomechanics,* Vol. 7*,* No. 1, pp. 1-15, DOI: 10.1061/(ASCE)1532-3641(2007)7:1(1).

Coulomb, C. A. (1776). "Essai sur une application des règles de maximis & minimis à quelques problèmes de statique, relatifs à l'architecture." *De l'Imprimerie Royale*.

Graham, J. (1971). "Calculation of passive pressure in sand." *Canadian Geotechnical Journal,* Vol. 8*,* No. 4, pp. 566-578, DOI: 10.1139/t71-058.

Haar, A. and Karman, T. V. (1909). "Zur Theorie der Spannungszustände in plastischen und sandartigen Medien." *Nachrichten von der Gesellschaft der Wissenschaften zu Göttingen, Mathematisch-Physikalische Klasse,* Vol. 1909*,* pp. 204-218.

Hettiaratchi, D. and Reece, A. (1975). "Boundary wedges in two-dimensional passive soil failure." *Geotechnique,* Vol. 25*,* No. 2, pp. 197-220, DOI: 10.1680/geot.1975.25.2.197.

Jahanandish, M. and Keshavarz, A. (2005). "Seismic bearing capacity of foundations on reinforced soil slopes." *Geotextiles and Geomembranes* Vol. 23*,* No. 1, pp. 1-25, DOI: 10.1016/j.geotexmem.2004.09.001.

Kérisel, J. and Absi, E. (1990). "Tables for the calculation of passive pressure, active pressure and bearing capacity of foundations." *Gauthier-Villard, Paris*.

Keshavarz, A. (2016). "Evaluation of the plastic critical depth in seismic active lateral earth pressure problems using the stress characteristics method." *Acta Geotechnica Slovenica,* Vol. 13*,* No. 1, pp. 19-27.

Keshavarz, A. and Ebrahimi, M. (2016). "The effects of the soil-wall adhesion and friction angle on the active lateral earth pressure of circular retaining walls." *International Journal of Civil Engineering,* Vol. 14*,* No. 2, pp. 97-105, DOI: 10.1007/s40999-016-0016-3.

Keshavarz, A., Fazeli, A., and Sedeghi, S. (2016). "Seismic bearing capacity of strip footings on rock masses using the Hoek-Brown failure criterion." *Journal of rock mechanics and Geotechnical Engineering,* Vol. 8, No. 2, pp. 170-177, DOI: 10.1016/j.jrmge.2015.10.003.

Keshavarz, A., Jahanandish, M., and Ghahramani, A. (2011). "Seismic bearing capacity analysis of reinforced soils by the method of stress characteristics." *Iranian Journal of Science and Technology-Transactions of Civil Engineering,* Vol. 35*,* No. C2, pp. 185-197.

Kumar, J. (2001). "Seismic passive earth pressure coefficients for sands." *Canadian Geotechnical Journal,* Vol. 38*,* No. 4, pp. 876-881, DOI: 10.1139/t01-004.

Kumar, J. and Chitikela, S. (2002). "Seismic passive earth pressure coefficients using the method of characteristics." *Canadian Geotechnical Journal,* Vol. 39, No. 2, pp. 463-471, DOI: 10.1139/t01-103.

Kumar, J. and Subba Rao, K. (1997). "Passive pressure coefficients, critical failure surface and its kinematic admissibility." *Geotechnique,* Vol. 47, No. 1, pp. 185-192, DOI: 10.1680/geot.1997.47.1.185.

Lee, I. and Herington, J. (1972). "A theoretical study of the pressures acting on a rigid wall by a sloping earth or rock fill." *Geotechnique,* Vol. 22, No. 1, pp. 1-26, DOI: 10.1680/geot.1972.22.1.1.

Liu, F. (2014). "Lateral earth pressures acting on circular retaining walls." *International Journal of Geomechanics* Vol. 14, No. 3, pp. 04014002, DOI: 10.1061/(ASCE)GM.1943-5622.0000291.

Liu, F. and Wang, J. (2008). "A generalized slip line solution to the active earth pressure on circular retaining walls." *Computers and Geotechnics,* Vol. 35*,* No. 2, pp. 155-164, DOI: 10.1016/j.compgeo.2007.06.002.

Liu, F., Wang, J., and Zhang, L. (2008). "Axi-symmetric active earth pressure for layered backfills obtained by the slip line method." *Journal of Shanghai Jiaotong University (Science),* Vol. 13, pp. 579-584, DOI: 10.1007/s12204-008-0579-5.

Liu, F., Wang, J., and Zhang, L. (2009a). "Analytical solution of general axisymmetric active earth pressure." *International Journal for Numerical and Analytical Methods in Geomechanics* Vol. 33*,* No. 4, pp. 551-565, DOI: 10.1002/nag.736.

Liu, F., Wang, J., and Zhang, L. (2009b). "Axi-symmetric active earth pressure obtained by the slip line method with a general tangential stress coefficient." *Computers and Geotechnics,* Vol. 36, No. 1, pp. 352-358, DOI: 10.1016/j.compgeo.2008.02.002.

Lu, H. and Yuan, B. (2011). "Calculation of passive earth pressure of cohesive soil based on Culmann's method." *Water Science and Engineering,* Vol. 4*,* No. 1, pp. 101-109, DOI: 10.3882/j.issn.1674-2370.2011.01.010.

Martin, C. (2005). "Exact bearing capacity calculations using the method of characteristics." *Proc. IACMAG Turin,* pp. 441-450.

Patki, M. A., Mandal, J. N., and Dewaikar, D. M. (2015). "Computation of passive earth pressure coefficients for a vertical retaining wall

with inclined cohesionless backfill." *International Journal of Geo-Engineering,* Vol. 6, No. 1, pp. 1-17, DOI: 10.1186/s40703-015-0004-5.

Peng, M. X. and Chen, J. (2013). "Slip-line solution to active earth pressure on retaining walls." *Geotechnique,* Vol. 63, No. 12, pp. 1008-1019, DOI: 10.1680/geot.11.P.135.

Rankine, W. M. (1857). "On the stability of loose earth." *Philosophical Transactions of the Royal Society of London,* Vol. 147, pp. 9-27.

Reddy, N. S. C., Dewaikar, D., and Mohapatra, G. (2013). "Computation of passive earth pressure coefficients for a horizontal cohesionless backfill using the method of slices." *International Journal of Advanced Civil Engineering and Architecture Research,* Vol. 2, No. 1, pp. 32-41.

Shields, D. H. and Tolunay, A. Z. (1973). "Passive pressure coefficients by method of slices." *Journal of the Soil Mechanics and Foundations Division,* Vol. 99, No. 12, pp. 1043-1053.

Sokolovskii, V. V. (1960). "Statics of soil media." *Butterworths Scientific Publications*.

Sokolovskii, V. V. (1965). "Statics of granular media." *Pergamon*.

Soubra, A. H. (2000). "Static and seismic passive earth pressure coefficients on rigid retaining structures." *Canadian Geotechnical Journal,* Vol. 37, No. 2, pp. 463-478, DOI: 10.1139/t99-117.

Soubra, A. H. and Macuh, B. (2002). "Active and passive earth pressure coefficients by a kinematical approach." *Proceedings of the ICE-Geotechnical Engineering,* Vol. 155, No. 2, pp. 119-131, DOI: 10.1680/geng.2002.155.2.119.

Terzaghi, K. (1943). "Theoretical soil mechanics." *John Wiley & Sons, Inc.* DOI: 10.1002/9780470172766.

Tobar, T. and Meguid, M. A. (2011). "Experimental study of the earth pressure distribution on cylindrical shafts." *Journal of Geotechnical and Geoenvironmental Engineering,* Vol. 137, No. 11, pp. 1121-1125, DOI: 10.1061/(ASCE)GT.1943-5606.0000535.

Tran, V. D., Meguid, M. A., and Chouinard, L. E. (2012). "Discrete element and experimental investigations of the earth pressure distribution on cylindrical shafts." *International Journal of Geomechanics* Vol. 14, No. 1, pp. 80-91, DOI: 10.1061/(ASCE)GM.1943-5622.0000277.

Veiskarami, M., Eslami, A., and Kumar, J. (2011). "End-bearing capacity of driven piles in sand using the stress characteristics method: Analysis and implementation." *Canadian Geotechnical Journal,* Vol. 48, No. 10, pp. 1570-1586, DOI: 10.1139/t11-057.

Veiskarami, M., Kumar, J., and Valikhah, F. (2014). "Effect of the flow rule on the bearing capacity of strip foundations on sand by the upper-bound limit analysis and slip lines." *International Journal of Geomechanics* Vol. 14, No. 3, pp. 04014008, DOI: 10.1061/(ASCE) GM.1943-5622.0000324.

Yang, K. H. and Liu, C. N. (2007). "Finite element analysis of earth pressures for narrow retaining walls." *Journal of GeoEngineering,* Vol. 2, No. 2, pp. 43-52.

Yap, S., Salman, F., and Shirazi, S. (2012). "Comparative study of different theories on active earth pressure." *Journal of Central South University,* Vol. 19, No. 10, pp. 2933-2939, DOI: 10.1007/s11771-012-1361-2.

Zhu, D. Y. and Qian, Q. (2000). "Determination of passive earth pressure coefficients by the method of triangular slices." *Canadian Geotechnical Journal,* Vol. 37, No. 2, pp. 485, DOI: 10.1139/t99-123.